Chemical Science

ROYAL SOCIETY OF CHEMISTRY

EDGE ARTICLE

Cite this: *Chem. Sci.*, 2021, **12**, 442

All publication charges for this article have been paid for by the Royal Society of Chemistry

A pH reversibly activatable NIR photothermal/photodynamic-in-one agent integrated with renewable nanoimplants for image-guided precision phototherapy†

Xu Zhao, *[abc] Kai-Chao Zhao,[cd] Li-Jian Chen,[abc] Yu-Shi Liu,[c] Jia-Lin Liu[cd] and Xiu-Ping Yan *[abcd]

Received 11th August 2020
Accepted 29th October 2020

DOI: 10.1039/d0sc04408c

rsc.li/chemical-science

Phototherapy has great potential to revolutionize conventional therapeutic modalities. However, most phototherapeutic strategies based on multicomponent therapeutic agents generally lack tumor-specificity, resulting in asynchronous therapy and superimposed side-effects. Severe heat damage is also inevitable because of the necessity of continuous external irradiation. Here we show the design of an acid-activated and continuous external irradiation-free photothermal and photodynamic (PTT/PDT) synchronous theranostic nanoplatform for precision tumor-targeting near-infrared (NIR) image-guided therapy. pH-reversibly responsive brominated asymmetric cyanine is designed as the tumor-specific NIR PTT/PDT-in-one agent to enhance anticancer efficiency and reduce side-effects. Ultra-small NIR persistent luminescence nanoparticles are prepared as both the imaging unit and renewable nanoimplant. Biotin functionalized polyethylene glycol is introduced to endow active tumor-targeting ability and prolong blood-circulation. The developed smart platform offers merits of reversible activation, PTT/PDT synergetic enhancement, tumor targetability and continuous external irradiation-free properties, allowing autofluorescence-free image-guided phototherapy only in tumor sites. This work paves the way to developing smart theranostic nanoplatforms for precision medicine.

Introduction

Phototherapy, a localized, spatiotemporally controllable and less invasive therapy tool, has great potential to revolutionize conventional therapeutic modalities for precision therapy.[1] Photothermal therapy (PTT) and photodynamic therapy (PDT), two modalities of phototherapy, produce local hyperthermia and generate cytotoxic reactive oxygen species (ROS), respectively, to induce cell apoptosis or even necrosis upon light excitation.[2–4] However, PTT and PDT are often plagued by the thermoresistance of cancer cells and inadequate oxygen supply in a hypoxic tumor microenvironment, respectively.[5–7] Thus, using PTT or PDT alone is difficult for efficient therapy. Although considerable efforts have been made to integrate PTT and PDT into one platform to improve therapeutic efficacy,[8–11] most PTT and PDT synergistic platforms are based on multi-component PTT and PDT agents,[11,12] resulting in asynchronous therapy and superimposed side-effects. Besides, conventional phototherapeutic agents are mostly in the "always on" state and lack tumor specificity, leading to severe nonspecific damage to normal tissue.[3,13,14] The therapeutic effect of conventional phototherapy also strongly depends on continuous external irradiation, inevitably causing severe overheating damage to normal tissue.[15,16] Hence, an enormous challenge remains in developing innovative smart activatable PTT and PDT integrated agents with precision tumor-targeting and efficient therapy. In this sense, exploring 'clean' excitation sources without nonspecific thermal damage is of particular significance.

Persistent luminescence nanoparticles (PLNPs) are magical optical materials that can store excitation energy and emit persistent luminescence after the cessation of excitation.[17–19] Besides, the luminescence of near-infrared (NIR) PLNPs can be reactivated with deep tissue penetrable NIR light, enabling detection and imaging without the need for continuous *in situ* excitation, thereby eliminating autofluorescence interference[20–22] and avoiding phototoxicity and tissue thermal damage from long-time continuous excitation.[23–26] PLNPs, therefore, are

[a]*State Key Laboratory of Food Science and Technology, Jiangnan University, Wuxi 214122, China. E-mail: zhaoxu2017@jiangnan.edu.cn; xpyan@jiangnan.edu.cn*

[b]*International Joint Laboratory on Food Safety, Jiangnan University, Wuxi 214122, China*

[c]*Institute of Analytical Food Safety, School of Food Science and Technology, Jiangnan University, Wuxi 214122, China*

[d]*Key Laboratory of Synthetic and Biological Colloids, Ministry of Education, School of Chemical and Material Engineering, Jiangnan University, Wuxi, 214122, China*

† Electronic supplementary information (ESI) available: Chemicals and materials, instrumentation, synthetic procedures, experimental details, ^{1}H and ^{13}C NMR data, mass spectra and other supplementary figures. See DOI: 10.1039/d0sc04408c

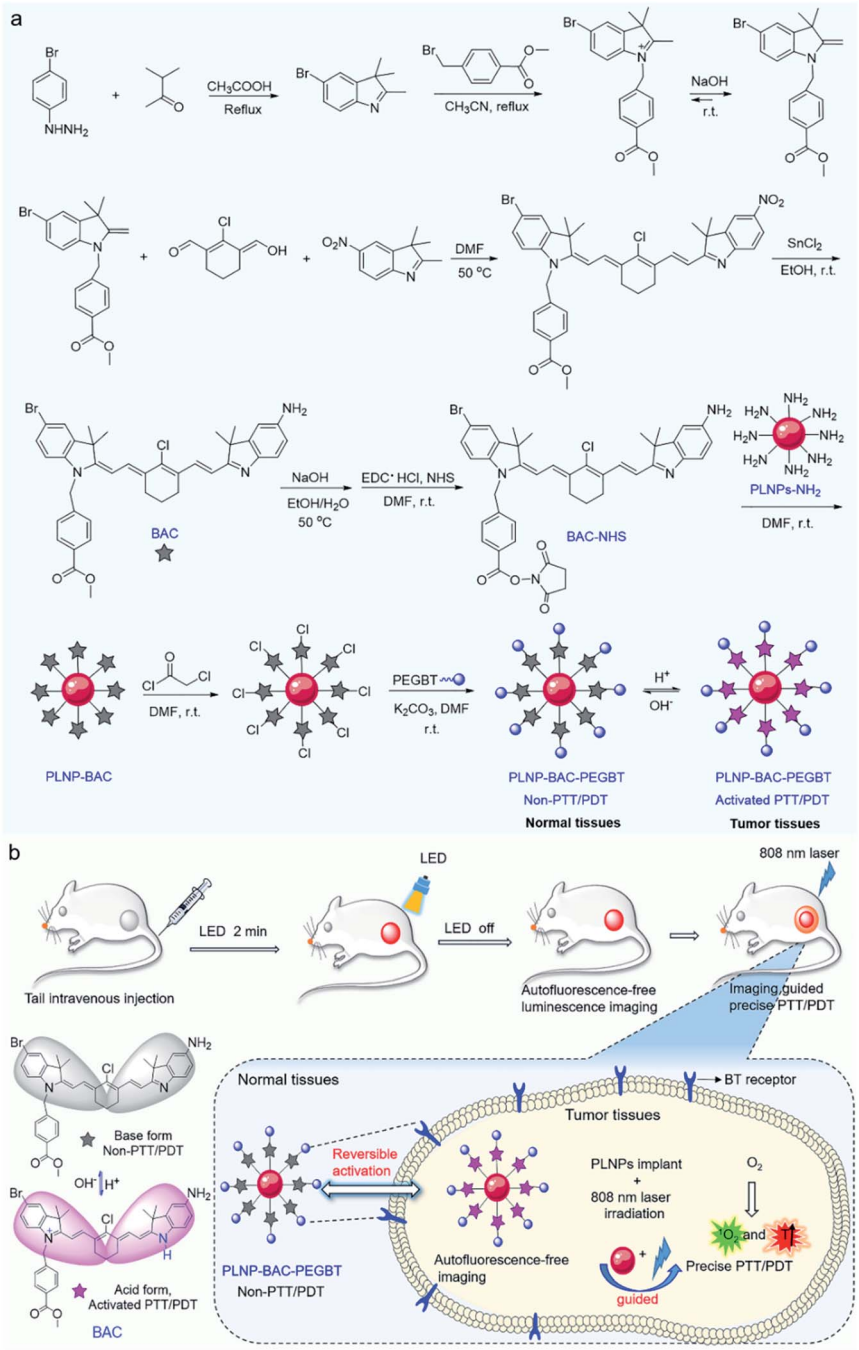

Fig. 1 Design of the PLNP-BAC-PEGBT theranostic platform. (a) Design strategy and synthetic route for BAC and PLNP-BAC-PEGBT. (b) Illustration of PLNP-BAC-PEGBT as a pH-reversibly activatable PDT/PTT synchronous theranostic platform for autofluorescence-free image-guided precision phototherapy without continuous external irradiation.

not only competent for long-term *in vivo* autofluorescence-free imaging, but also show tremendous promise in continuous external irradiation-free phototherapy. The great potential of PLNPs as a built-in light source to reduce the side-effects of PDT associated with continuous external irradiation has been revealed, but exclusively restricted to 'always on' PDT systems.[23–27] Besides, most PLNPs suffer from serious agglomeration or poor luminescence performance,[22,26,28–31] impeding further biomedical applications. So, it is still challenging to develop high-performance PLNPs with excellent persistent luminescence and controllable morphology. In particular, intelligent integration of high-performance PLNPs with a smart activatable PTT/PDT-in-one agent is of great significance for precision therapy.

Herein, we report a rational design of an NIR-emitting ultrasmall PLNP sensitized pH-reversibly activatable PTT/PDT-in-one agent for precision tumor-targeting and autofluorescence-free image-guided synchronous phototherapy without

continuous external irradiation. pH reversibly responsive brominated asymmetric cyanine (BAC) is designed as an activatable NIR PTT/PDT-in-one agent for precision tumor-targeting and high-efficiency therapy. Ultra small-sized monodispersed PLNPs with excellent NIR persistent luminescence are prepared as both the autofluorescence-free imaging unit and built-in light source to guide and trigger PDT/PTT. Meanwhile, biotin (BT) functionalized polyethylene glycol (PEGBT) is introduced into the PLNP sensitized pH reversibly activatable PTT/PDT-in-one nanoplatform (PLNP-BAC-PEGBT) to endow active tumor-targeting ability and prolong blood-circulation.[32,33] The as-prepared PLNP-BAC-PEGBT theranostic nanoplatform not only exhibits precision tumor-targeted imaging without autofluorescence interference, but also shows an ultra-strong PTT/PDT effect with excellent tumor-specificity and ignorable side-effects, holding great potential for precision medicine.

Results and discussion

Design of the PLNP-BAC-PEGBT theranostic nanoplatform

Fig. 1 shows the design strategy of the PLNP-BAC-PEGBT theranostic platform for autofluorescence-free image-guided precision tumor-targeting phototherapy without continuous external irradiation. To realize precision tumor-targeting and PTT/PDT synchronous efficient therapy, we design a non-*N*-alkylated BAC molecule as the pH-reversibly activatable PTT/PDT-in-one agent. Unsubstituted N atoms in the indole ring of BAC are employed as the specific recognition sites for the acid microenvironment to realize tumor-specific activation. The heavy atom Br is introduced to improve intersystem crossing (ISC) from the lowest excited singlet (S1) state to the lowest excited triplet (T1) state to enhance the ROS generation.[34,35] Meanwhile, a chemically active ester is introduced into BAC to integrate NIR-emitting PLNPs as a built-in excitation source for continuous external irradiation-free imaging and phototherapy. PEGBT is further introduced on the surface of the PLNP sensitized BAC theranostic platform (PLNP-BAC) with chloroacetyl chloride as bridges to endow active tumor-targeting ability and prolong blood-circulation (Fig. 1a). As such, the designed PLNP-BAC-PEGBT enables autofluorescence-free NIR imaging-guided precision tumor-targeting phototherapy with no need for continuous external irradiation.

Preparation and characterization of BAC

The synthetic route for the synthesis of BAC is illustrated in Fig. 1a while the synthesis procedures are detailed in the ESI. The structures of the synthesized BAC and the important intermediates were confirmed from the nuclear magnetic resonance, mass spectra and FT-IR spectra (Fig. S1–S14†). BAC presents a characteristic absorption peak at *ca*. 506 nm in a weakly basic medium (ethanol/water, 3/7 v/v; pH 7.4, simulated normal physiological pH), but shows a new shoulder band at *ca*. 783 nm with an evident decreased absorption band at 506 nm in a weakly acidic medium (pH 6.0, simulated tumor acidic microenvironment[36,37]) (Fig. 2a). Meanwhile, the BAC solution turns from pink to green because the protonation of the indole ring N atoms leads to the transition of BAC from its base form to its acid form and *vice versa* (Fig. S15†). The reversible characteristic absorption change of BAC with pH lays a solid foundation for pH-reversibly activatable PDT/PTT. Density functional theory (DFT) calculation shows that the protonation of the indole ring N atoms narrows the gap (E_g) between the highest occupied molecular orbital (HOMO) and the lowest unoccupied molecular orbital (LUMO) of BAC, leading to a distinct redshift of the absorption peak (Fig. 2b). Besides, the acidic environment enables the activation of the NIR fluorescence of BAC with a characteristic emission peak at 830 nm (Fig. 2a and S16a†) due to the protonation of the indole ring N atoms accompanied by the intramolecular change transfer process. The pK_a and the pH sensitive intervals of the synthesized BAC determined by means of fluorescence titration are 5.2 and 4.5–7.0, respectively (Fig. S16†). The results indicate that the as-synthesized BAC has pH reversible response features and tumor acidic microenvironment-matched pH sensitive intervals, providing great potential for tumor microenvironment specific activation.

We then investigated the photothermal and photodynamic performance of BAC. DFT calculation shows that the protonated BAC can be excited to the S1 state under 808 nm irradiation in the acidic microenvironment (Fig. 2c). The S1 state consumes its energy not only through a nonradiative decay pathway accompanied by heat release due to the strong ICT effect of the protonated BAC, but also *via* an enhanced ISC from the S1 state to the T1 state owing to the heavy atom effect. Meanwhile, energy transfer from the T1 state to triplet oxygen further occurs to yield singlet oxygen ($^1O_2$) (Fig. 2c). Hence, BAC has great potential for tumor acidic microenvironment specifically activated photothermal and photodynamic performance. The acid-activated photothermal effect of BAC at various power densities of 808 nm laser irradiation was evaluated first. The BAC solution exhibited an obvious increase of temperature at pH 6.0 and displayed power density and exposure time-dependent hyperthermia (Fig. 2d). The photothermal conversion performance of indocyanine green (ICG), approved by the United States Food and Drug Administration,[4,38–40] was also measured as a reference. Importantly, BAC showed a more obvious increase of temperature than ICG (with the same concentration and power density) (Fig. 2d), indicating that the as-prepared BAC at pH 6.0 has a superior photothermal effect. The photothermal conversion efficiency of BAC at 0.6 W cm^{-2} of 808 nm irradiation was calculated to be 37.9% (Fig. S17†). In comparison, the control groups, phosphate buffer solution (PBS, pH 7.4) and BAC at pH 7.4, did not trigger any increase of temperature even if the power density and exposure time were up to 0.6 W cm^{-2} and 10 min, respectively (Fig. 2d). These results clearly show that the photothermal effect of BAC could be switched on only in an acidic microenvironment, making it qualified for tumor acidic microenvironment specifically activated PTT. Besides, BAC has much higher photostability than ICG, especially at pH 7.4 (Fig. 2e, S18 and S19†), ensuring strong stability in blood circulation and therapy. Considering both photothermal efficiency and the photobleaching effect, 0.6 W cm^{-2} was taken as the irradiating power in the follow-up study.

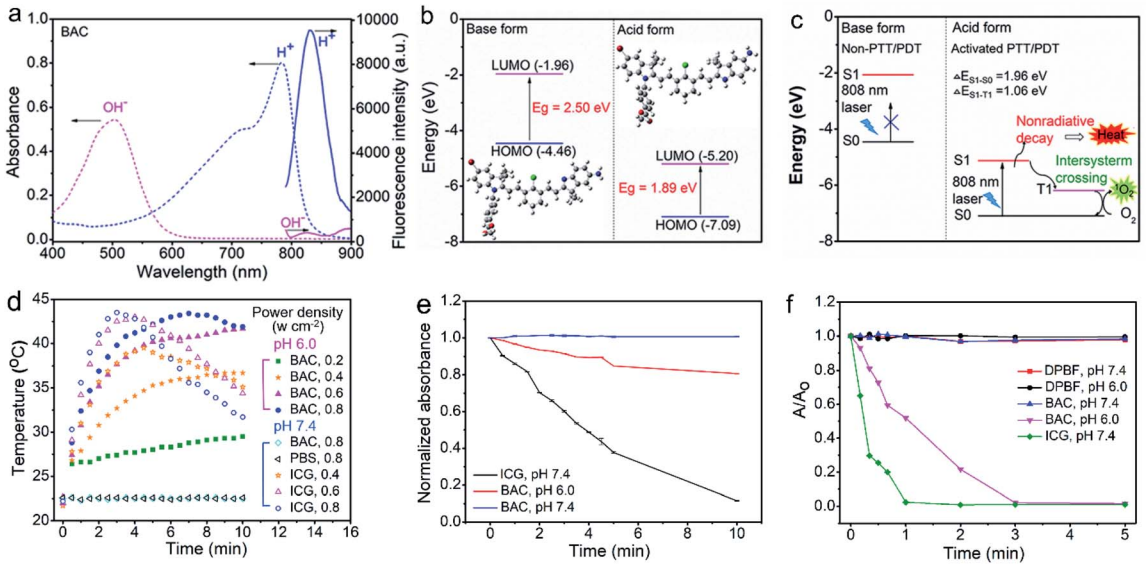

Fig. 2 Characterization of BAC. (a) UV-vis-NIR absorption (dotted lines) and fluorescence (solid lines) spectra of BAC at pH 6.0 (blue lines) and 7.4 (magenta lines). (b) Optimized structures and frontier molecular orbital (HOMO and LUMO) energies from DFT calculations (Gaussian 09/6-31G (d)) of BAC in its ground state (S0). (c) Illustration for photothermal and $^1O_2$ generation of BAC. (d) Time dependent temperature of BAC at pH 6.0 and 7.4 and ICG at pH 7.4 under continuous 808 nm laser irradiation with different power densities. (e) Effect of irradiation time on the absorbance of BAC at pH 7.4 or 6.0 and ICG at pH 7.4 at the corresponding maximum absorption wavelength. (f) Time-dependent absorbance of DPBF (A/A_0) at 410 nm without and with BAC or ICG at pH 6.0 and 7.4 under continuous 808 nm laser irradiation. A_0 is the initial absorbance of DPBF, while A is the absorbance of DPBF at a certain irradiation time.

The acid-activated photodynamic effect of BAC was evaluated further under various power densities of 808 nm laser irradiation. The $^1O_2$ generation efficiency of BAC at pH 7.4 or 6.0 under 808 nm laser was measured with 1,4-diphenyl-2,3-benzofuran (DPBF) as the $^1O_2$ probe. The decrease in the absorbance of DPBF due to $^1O_2$ oxidation was used to evaluate the relative generation efficiency of $^1O_2$. DBPF alone is stable during 5 min of continuous irradiation using an 808 nm laser (0.6 W cm^{-2}) (Fig. 2F and S20†). The negligible reduction of the absorbance of DPBF indicates that BAC at pH 7.4 under the same laser irradiation did not produce $^1O_2$ (Fig. 2f and S21a†). However, BAC at pH 6.0 under the same laser irradiation generated significant $^1O_2$ as confirmed by the rapid decrease of the absorbance of DPBF (Fig. 2f and S21b†). In contrast, ICG enabled $^1O_2$ generation at pH 7.4 under the same irradiation (Fig. 2f and S22†). The distinct feature of BAC for the efficient generation of $^1O_2$ only in an acidic environment indicates that BAC is also promising for tumor-specific PDT. The unique pH reversible response activation and weak acidity specifically activated PTT/PDT effect provide BAC with great potential as a smart activatable PTT/PDT-in-one agent for tumor-targeting precision phototherapy.

Preparation and characterization of PLNPs

Ultra-small sized PLNPs with excellent NIR persistent luminescence and super-long afterglow are the fundamental requirements of *in vivo* imaging and the built-in excitation source. However, traditional preparation methods hardly provide a compromise between the small size and excellent luminescence performance. Besides, most of the available PLNPs need UV light excitation to produce persistent luminescence and have limited ability to reactivate the persistent luminescence with visible and NIR light, which is unfavourable for long-term *in vivo* application.[26] In a previous report, we proposed a surfactant-aided hydrothermal method in combination with a short term calcination method to prepare monodispersed triple-doped NIR PLNPs (*ca.* 40 nm) with bright luminescence and red LED light or 808 nm laser renewable feature,[26,28] but gradient centrifugation was still inevitable to obtain the small-sized nanoparticles, leading to low yield. Here we show the preparation of ultra-small size, ultra-bright and NIR light renewable PLNPs with no need for gradient centrifugation *via* careful control of the hydrothermal and calcination conditions (Fig. S23†). The doping elements and doping ratio are consistent with the stoichiometry of the chemical formula ($Zn_{1.25}Ga_{1.5}Ge_{0.25}O_4$:0.5%$Cr^{3+}$,2.5%$Yb^{3+}$,0.25%$Er^{3+}$) in our previous work.[26,28] The solvothermal method with a high-temperature and long time (220 °C, > 24 h) in combination with low-temperature calcination (800 °C, 1 h) significantly improved the optical performance of the PLNPs with no obvious agglomeration (Fig. S23†). Our improved method yielded ultra-small sized, mono-dispersed and NIR light renewable PLNPs with an average diameter of 12.8 ± 1.1 nm (calculated from 100 randomly selected particles) and a uniform lattice spacing of 0.24 nm without further gradient centrifugation (Fig. S24a and b†).

The as-prepared PLNPs gave an NIR $^2E \rightarrow {}^4A_2$ luminescence emission peak from 650 to 900 nm (Fig. S24c†). The overlap between the luminescence emission peak of the as-prepared PLNPs and the absorption peak of the synthesized BAC in its

acid form enables the PLNPs to sensitize BAC based on Förster resonance energy transfer (FRET). Besides, the PLNPs exhibited super long-lasting and repeatable NIR afterglow upon pre-excitation with 254 nm UV light (Fig. S24d and g†). Interestingly, the persistent luminescence of the PLNPs can be reactivated with 650 nm red LED light and 808 nm laser irradiation (Fig. S24e and f†) *via* a photo-assisted excitation process.[26,41] These unique optical properties and ultra-small size make the as-prepared PLNPs qualified for long-term autofluorescence-free *in vivo* imaging and as a renewable built-in light source for continuous external irradiation-free PTT and PDT.

Preparation and characterization of the PLNP-BAC-PEGBT theranostic nanoplatform

The above results encouraged us to employ the prepared BAC and PLNPs to construct a PLNP sensitized BAC theranostic platform for autofluorescence-free image-guided precision tumor-targeting phototherapy without continuous external irradiation. To enhance its reaction activity, BAC was first hydrolyzed and then reacted with 1-ethyl-3-(3-dimethylaminopropyl) carbodiimide hydrochloride (EDC·HCl) and *N*-hydroxysuccinimide (NHS) *via* amide condensation to yield the active succinimide ester of BAC (BAC-NHS) (Fig. 1a). Amino functionalized PLNPs (PLNP-NH_2) were then obtained (Fig. S25†) to covalently bond with BAC-NHS *via* ester-amide condensation to form the PLNP sensitized activatable PTT/PDT-in-one theranostic platform (PLNP-BAC). To endow active tumor-targeting ability and prolong blood-circulation, PEGBT was further introduced onto the surface of PLNP-BAC with chloroacetyl chloride as a bridge. For this purpose, PLNP-BAC was modified with chloroacetyl chloride to yield PLNP-BAC-Cl *via* an acylation reaction between the –NH_2 group of PLNP-BAC and the –COCl group of chloroacetyl chloride with potassium carbonate as the deacid reagent. The obtained PLNP-BAC-Cl had a terminal –CH_2Cl group to further react with PEGBT *via* nucleophilic substitution to produce PEGBT modified PLNP-BAC (PLNP-BAC-PEGBT) (Fig. 1a). As such, a smart theranostic platform PLNP-BAC-PEGBT was successfully constructed.

Conjugation of BAC and PEGBT did not lead to obvious morphological change or significant aggregation of PLNP-NH_2 (Fig. 3a *vs.* Fig. S24a†), but remarkably increased the hydrodynamic size of PLNP-NH_2 from 58.9 ± 2.3 nm to 91.6 ± 3.2 nm and 122.2 ± 3.7 nm, respectively, owing to the conjugated rigid plane structure of BAC and the large hydrodynamic volume of PEGBT (Fig. 3b). Meanwhile, the zeta potential turned from 12.67 ± 4.38 mV to 11.63 ± 3.48 and −16.97 ± 3.24 mV, respectively (Fig. 3c). The disappearance of the characteristic bands at 3241 cm^{-1} (–NH_2 stretching vibration of PLNPs) and 1703 cm^{-1} (–COOH stretching vibration of BAC) in conjunction with the appearance of the characteristic peaks at 1650 cm^{-1} (stretching vibration of –CONH–) and 1600–1450 cm^{-1} (stretching vibration of the benzene skeleton) in the FT-IR spectrum of PLNP-BAC-PEGBT also confirm the successful conjugation of BAC and PEGBT onto the PLNPs (Fig. 3d). The color of PLNP-BAC turned from white to pink (color of BAC in its base form) further indicates the presence of BAC on the surface of PLNPs (Fig. S26†). The content of BAC conjugated onto the surface of PLNPs was measured to be 1.3×10^{-4} mol g^{-1} *via* UV-vis-NIR absorption spectrometry. In addition, the prepared PLNP-BAC-PEGBT gave a pure spinel phase of $ZnGa_2O_4$ and Zn_2GeO_4 (JCPDS file number 38-1240 and 25-1018, respectively) like PLNPs (Fig. 3e), indicating no crystal phase change during the whole functionalization process.

Conjugation of BAC and PEGBT to PLNPs had an insignificant effect on the inherent luminescence intensity and the persistent luminescence of PLNPs at pH 7.4 (Fig. 3f, S26 and S27b†). The change of pH from 7.4 to 6.0 slightly decreased the luminescence intensity and persistent luminescence (Fig. 3f and S27†) owing to the FRET effect from PLNPs to BAC originating from the overlap between the absorption peak of BAC in its acid form and the emission peak of PLNPs. Even so, the luminescence of PLNP-BAC-PEGBT was still clearly observed using the *in vivo* imaging system (Fig. 3g). These results also show that the FRET process between PLNPs and BAC occurs if and only if a tumor acidic microenvironment is present, making smart tumor-specific PDT/PTT therapy *via* PLNPs as the built-in excitation light source possible.

In vitro PTT/PDT performance of PLNP-BAC-PEGBT

To reveal the synergistic acid-activated and continuous external irradiation-free photothermal effect of PLNP-BAC-PEGBT, continuous 808 nm laser irradiation as well as fractionated 808 nm laser irradiation (repeated cycles for 1 min laser on/1 min laser off) was carried out at 0.6 W cm^{-2}. An obvious temperature increase of PLNP-BAC-PEGBT was observed under both continuous and fractionated irradiation at pH 6.0 (Fig. 3h). In comparison, a slight temperature fluctuation was noted for BAC at pH 6.0 under fractionated 808 nm laser irradiation (Fig. 3h). Besides, naked PLNPs (either at pH 6.0 or pH 7.4) or PLNP-BAC-PEGBT (pH 7.4) only did not trigger any notable temperature increase upon 808 nm laser irradiation up to 10 min (Fig. 3h and S28†). The above results show that the as-prepared PLNP-BAC-PEGBT has great potential for tumor-specific PTT and PLNPs can act as a built-in light source for repeatable PTT due to their long NIR afterglow.

The $^1O_2$ generation performance of PLNP-BAC-PEGBT at pH 7.4 or 6.0 under continuous and fractionated 808 nm laser irradiation was then tested with DPBF as the probe for $^1O_2$. PLNP-BAC-PEGBT at pH 6.0 generated significant $^1O_2$ under continuous irradiation as confirmed by significant and rapid reduction of the absorbance of DPBF (Fig. 3i and S29b†). Interestingly, fractionated 808 nm laser irradiation of PLNP-BAC-PEGBT (pH 6.0) gave an $^1O_2$ generation efficiency similar to continuous irradiation in a period of 10 min (Fig. 3i). In contrast, PLNP-BAC-PEGBT at pH 7.4 under the same continuous or fractionated irradiation did not produce any $^1O_2$ as verified by negligible reduction of the absorbance of DPBF (Fig. 3i and S29a†). The above results clearly indicate that the as-prepared PLNP-BAC-PEGBT has excellent potential for tumor-specific PDT, and PLNPs are promising as the built-in light source for assisted enhanced PDT.

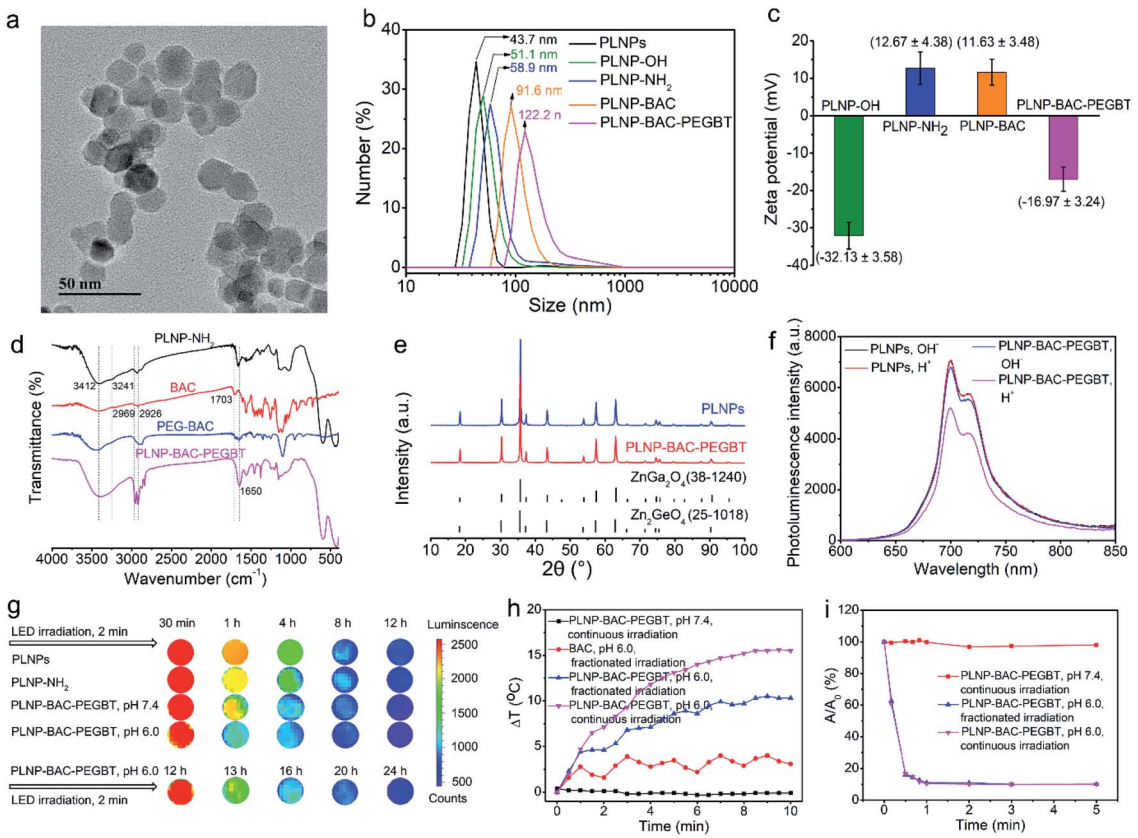

Fig. 3 Characterization of PLNP-BAC-PEGBT. (a) TEM images of PLNP-BAC-PEGBT. (b) Hydrodynamic diameter distribution of PLNPs, PLNP-OH, PLNP-NH_2, PLNP-BAC and PLNP-BAC-PEGBT. (c) Zeta potentials of PLNP-OH, PLNP-NH_2, PLNP-BAC and PLNP-BAC-PEGBT. (d) FT-IR spectra of PLNP-NH_2, BAC, PEGBT and PLNP-BAC-PEGBT. (e) XRD patterns of PLNPs, PLNP-BAC-PEGBT, $ZnGa_2O_4$ and Zn_2GeO_4. (f) Photoluminescence spectra of PLNPs and PLNP-BAC-PEGBT at pH 6.0 and 7.4. (g) Reactivated NIR persistent luminescence images of PLNPs, PLNP-NH_2 and PLNP-BAC-PEGBT at pH 7.4 and 6.0 recorded on a PerkinElmer IVIS Lumina III imaging system. (h) Irradiation time dependent temperature change curves of BAC and PLNP-BAC-PEGBT at pH 6.0 with continuous or fractionated 808 nm laser irradiation. (i) Time-dependent absorbance of DPBF (A/A_0) at 410 nm with PLNP-BAC-PEGBT at pH 6.0 and 7.4 under continuous or fractionated 808 nm laser irradiation. A_0 is the initial absorbance of DPBF, while A is the absorbance of DPBF at a certain irradiation time.

Cell targeting NIR imaging and PTT/PDT

The potential of PLNP-BAC-PEGBT for *in vitro* cell targeting luminescence imaging and PTT/PDT was demonstrated with HeLa and A549 cells, two kinds of biotin overexpressed cancer cells,[42–44] as model cells and biotin receptor-negative 3T3 cells as the negative control.[44] The cytotoxicity of PLNP-BAC-PEGBT towards the above cells was first evaluated *via* the MTT assay. The cell viability of these cells remained over 95% after 24 h of incubation even if the test concentration was up to 500 mg mL^{-1}, demonstrating negligible cytotoxicity and good biocompatibility of PLNP-BAC-PEGBT (Fig. S30 and S31†).

Cell internalization and imaging of PLNP-BAC-PEGBT were then investigated to show its targeting capability. To this point, 75 mg mL^{-1} PLNP-BAC-PEGBT was incubated with HeLa, A549 and 3T3 cells, respectively, and cell internalization was monitored using a confocal laser scanning microscope (CLSM). The luminescence signal in A549 cells incubated with PLNP-BAC-PEGBT was clearly brighter than that in BT pre-treated A549 cells or the A549 cells treated with PLNPs (control groups) although the same amount of PLNP-BAC-PEGBT (as PLNPs) was used (Fig. 4a), indicating that the BT on the surface of PLNP-BAC-PEGBT exhibits active targeting specificity and enhances the internalization of the nanoprobe. Besides, the BT mediated active tumor-targeting effect of PLNP-BAC-PEGBT was verified and quantified by flow cytometry analysis (Fig. S32†). The mean fluorescence intensity (MFI) of the cells incubated with PLNP-BAC-PEGBT exhibited about a 1.4-fold increase compared with that of the control groups. Furthermore, the CLSM and flow cytometry analysis of HeLa cells gave the same results (Fig. S33 and S34†). However, no noticeable difference in the results of CLSM and flow cytometry was observed in 3T3 cells treated with PLNPs or PLNP-BAC-PEGBT (Fig. S35 and S36†). These results clearly indicate that the internalization of PLNP-BAC-PEGBT by tumor cells was significantly improved by BT due to the enhanced permeation and retention effect and BT receptor mediated active tumor-targeting effect.

The photothermal and photodynamic cytotoxicity of PLNP-BAC-PEGBT was tested on tumor cells (A549 and HeLa, pH 6.0) and normal cells (3T3, pH 7.4). PLNP-BAC-PEGBT irradiated with an 808 nm laser exhibited obvious cytotoxicity against the tumor cells in an irradiation time dependent manner

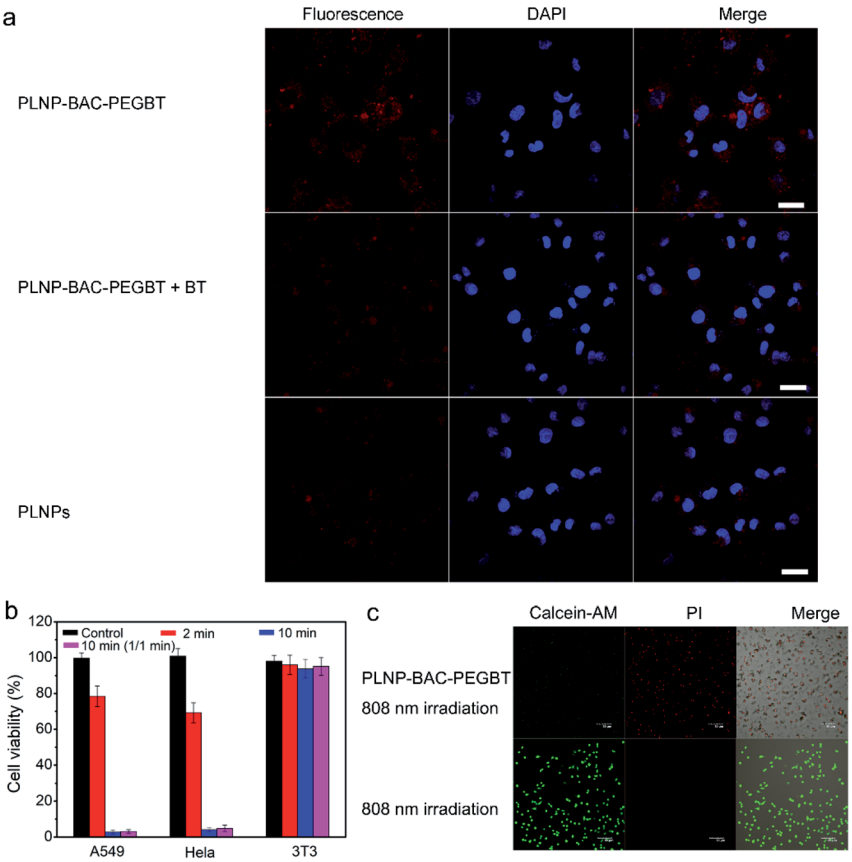

Fig. 4 Cell cytotoxicity and internalization of PLNP-BAC-PEGBT. (a) Cell internalization and cell imaging of PLNP-BAC-PEGBT toward A549 cells (scale bar, 30 μm). (b) Cell viability of PLNP-BAC-PEGBT with continuous or fractionated 808 nm laser irradiation against A549, HeLa and 3T3 cells. Control refers to continuous 808 nm laser irradiation (0.6 W cm^{-2}, 10 min); 2 min and 10 min refer to 2 min and 10 min continuous 808 nm laser irradiation (0.6 W cm^{-2}) with PLNP-BAC-PEGBT, respectively; 10 min (1/1 min) represents fractionated 808 nm laser irradiation (repeated cycles for 1 min laser on/1 min laser off, 0.6 W cm^{-2}) with PLNP-BAC-PEGBT for a total time of 10 min. (c) CLSM imaging of A549 cells incubated with or without PLNP-BAC-PEGBT under 10 min of 808 nm laser irradiation (0.6 W cm^{-2}) (Calcein-Am and PI staining).

(Fig. 4b, c and S37†). An extremely low cell viability (*ca.* 5%) was observed for A549 and HeLa cells treated with PLNP-BAC-PEGBT under continuous or fractionated 808 nm laser irradiation for a total time of 10 min (Fig. 4b, c, and S37†). In contrast, PLNP-BAC-PEGBT did not induce discernible cytotoxicity against 3T3 cells (cell viability *ca.* 90%) under all the above irradiation conditions, because the PTT/PDT effect of PLNP-BAC-PEGBT was inactive in normal cells (Fig. 4b and S38†). These results show that PLNPs can act as an efficient built-in light source for triggering PTT/PDT with no need for continuous external light irradiation and the PTT/PDT effect of PLNP-BAC-PEGBT could merely be activated in an acidic microenvironment, ensuring synergistic efficient therapy without side-effects to adjacent normal tissues.

In vivo autofluorescence-free tumor-targeting NIR imaging and precision therapy

The excellent biocompatibility, cell-targeting imaging and high-efficiency *in vitro* anti-tumor effect of PLNP-BAC-PEGBT encouraged us to explore whether it is suitable for *in vivo* autofluorescence-free tumor-targeting NIR imaging and image-guided precision phototherapy. The *in vivo* precision tumor-targeting imaging performance of PLNP-BAC-PEGBT was demonstrated through intravenously injecting PLNP-BAC-PEGBT (experimental group) or PLNP-BAC (control group) into HeLa tumor-bearing mice (Fig. 5a). The luminescence signal appeared at the tumor site of the experimental group at *ca.* 4 h, gradually increased to the maximum at *ca.* 6 h, and remained clear up to at least 12 h, indicating that the maximum amount of PLNP-BAC-PEGBT was accumulated in the tumor site at 6 h after injection. Hence, 6 h post-injection was chosen as the most appropriate time point for follow-up therapy. In contrast, almost no luminescence signal appeared at the tumor site of the control group, while the luminescence signal in the liver and lungs in the control group was slightly weaker than that in the experimental group, confirming that the introduction of PEGBT is indeed helpful in enhancing the tumor-targeting accumulation and prolonging the blood circulation time. Besides, autofluorescence background was effectively avoided during the imaging process because the imaging signal was acquired with no need for *in situ* excitation by taking advantage of the persistent luminescence feature. The above results confirm that PLNP-BAC-PEGBT has great potential for *in vivo*

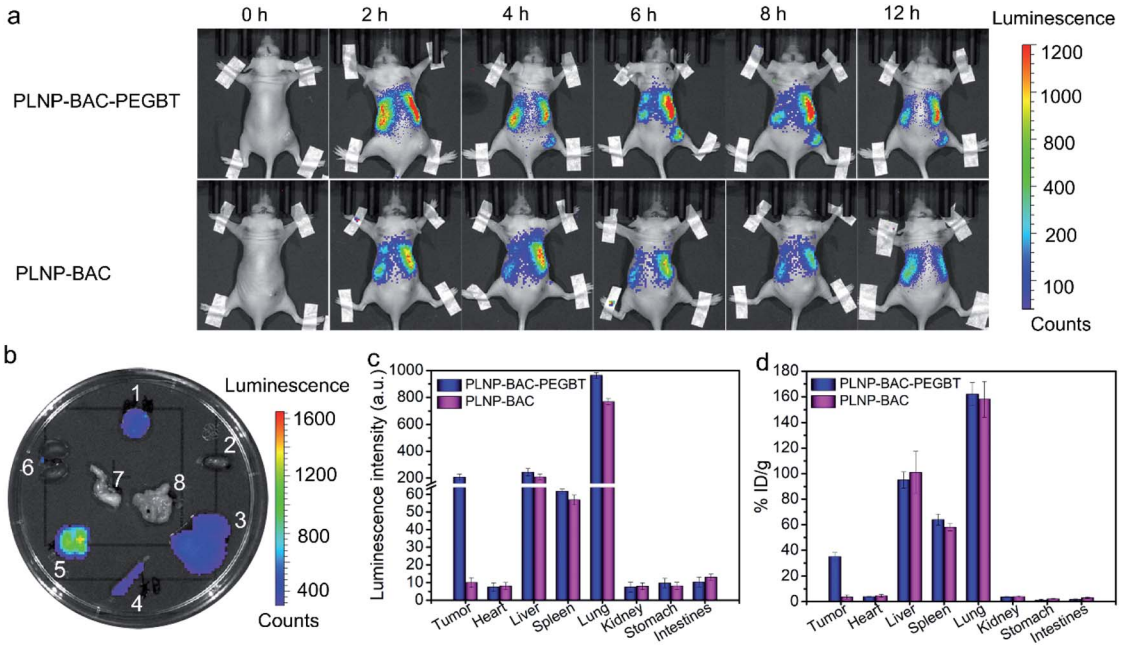

Fig. 5 PLNP-BAC-PEGBT-mediated *in vivo* luminescence images in HeLa tumor-bearing mice. (a) *In vivo* persistent luminescence imaging of HeLa tumor-bearing mice after intravenous injection with PLNP-BAC-PEGBT or PLNP-BAC pre-irradiated with a 254 nm UV light for 10 min before injection and irradiated with 650 nm LED light for 2 min before acquisition. (b) *Ex vivo* persistent luminescence images of the major organs and the tumor dissected from the mice at 6 h post-injection with PLNP-BAC-PEGBT (1–8: tumor, heart, liver, spleen, lungs, kidneys, stomach and intestines, respectively). (c) Luminescence intensity of the major organs and the tumor dissected from mice at 6 h after intravenous injection with PLNP-BAC-PEGBT or PLNP-BAC. (d) Biodistribution of PLNP-BAC-PEGBT or PLNP-BAC in the main organs and the tumor of the mice by measuring the content of the Zn element from PLNPs at 6 h after injection. The corresponding main organs and tumor tissue of HeLa tumor-bearing mice without any treatment were collected and measured as blank. Center values and error bars are defined as mean and s.d., respectively ($n = 3$).

autofluorescence-free tumor-targeting imaging and guiding the stimulus in the best time and at the accurate location.

The major organs and the tumor tissues were then collected at 6 h post intravenous injection for *ex vivo* imaging to further investigate the tumor-targeting accumulation and biodistribution (Fig. 5b and c). Although the luminescence signal in the lungs and liver and a slight luminescence signal in the spleen were inevitable due to the strong phagocytosis of reticuloendothelial system organs, a noticeable luminescence signal existed at tumor sites only in the PLNP-BAC-PEGBT group, further showing that the tumor-targeting accumulation was specifically improved by PEGBT. Moreover, the tumor-targeting accumulation of PLNP-BAC-PEGBT was confirmed by inductively coupled plasma mass spectrometry for the determination of Zn (originating from the PLNP core) in major organs and tumor tissues 6 h after the injection as well (Fig. 5d). The quantitative results further indicate that the PLNP-BAC-PEGBT group has higher tumor-targeting accumulation than PLNP-BAC, making PLNP-BAC-PEGBT promising for tumor-targeting accumulation and autofluorescence-free tumor-specific imaging.

We then evaluate the *in vivo* precision PTT/PDT of PLNP-BAC-PEGBT. Tumor-bearing mice were intravenously injected with PLNP-BAC-PEGBT and subjected to continuous or fractionated (repeated cycles for 1 min laser on/1 min laser off) 808 nm laser exposure (0.6 W cm^{-2} for a total time of 10 min) at 6 h post-injection as the treatment groups, while other tumor-bearing mice without any treatment or treated with PBS in combination with continuous/fractionated laser irradiation or PLNP-BAC-PEGBT only set as the control groups. The treatment group under continuous 808 nm laser exposure shows an obvious temperature increase in tumor sites (from the initial 32.5 °C to 49 °C) (Fig. S39†). Importantly, the treatment group under fractionated irradiation exhibits almost the same thermal increase (Fig. S39†), suggesting that the PLNP core can act as an effective built-in light for tumor PTT/PDT. In contrast, all control groups did not induce any increase of temperature (Fig. S39†), indicating that the photothermal effect of PLNP-BAC-PEGBT was specifically governed by the tumor acidic microenvironment and the 0.6 W cm^{-2} laser irradiation power (continuous or fractionated exposure) was acceptable with no obvious photothermal side-effects itself. Further experiments with a high power laser demonstrate that fractionated laser irradiation can effectively reduce damage of the laser itself compared with the traditional continuous irradiation (Fig. S40†).

A time-dependent change in tumor volume indicates that tumor tissues are obviously suppressed and disappear in the late-stage for PLNP-BAC-PEGBT with continuous or fractionated laser irradiation treatment groups, whereas the tumor tissues still increased significantly in the above control groups (Fig. 6a and b). To further investigate the *in vivo* therapeutic effect and

mechanism of PLNP-BAC-PEGBT under laser irradiation, histological and immunohistochemical (IHC) analyses (including Ki67 and cleaved caspase 3 for cell proliferation and apoptosis, respectively) of tumor tissue slices were carried out at 24 h post treatment. The hematoxylin and eosin (H&E) staining results show that the tumor tissues in treatment groups were seriously damaged with obvious karyopyknosis and many void spaces of tumor cells in comparison with the control groups (Fig. S41†). Meanwhile, the treatment groups showed obvious inhibition of cell proliferation and significant promotion of apoptosis as confirmed by the obvious decrease of the expression of Ki67 and the increase of caspase 3 (Fig. S42†), which is consistent with the observed tumor tissue inhibition or even disappearance. Furthermore, the systemic toxicity of the PLNP-BAC-PEGBT platform was also evaluated by histology analysis after the treatment process, where no obvious organ damage

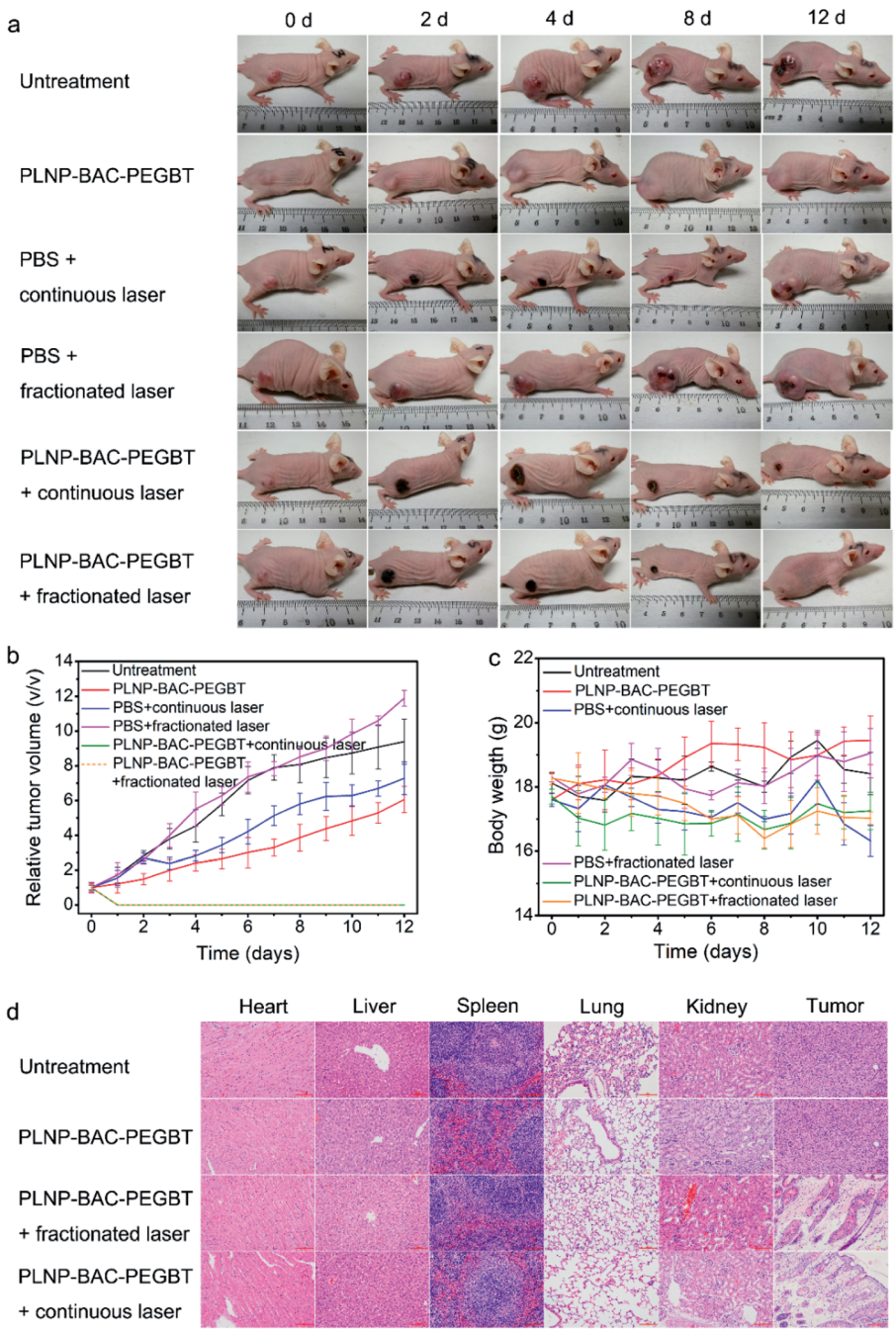

Fig. 6 PLNP-BAC-PEGBT-mediated *in vivo* PTT/PDT in HeLa tumor-bearing mice models. (a) Representative photos for different groups of mice during the PTT/PDT therapy process. (b) Tumor volume change in mice during the PTT/PDT process relative to initial tumor volumes. (c) Body weight change of mice during the PTT/PDT process. (d) H&E staining of the main organs and tumor tissues of mice after the treatment (scale bar, 100 μm). Center values and error bars are defined as mean and s.d., respectively ($n = 3$).

and inflammation were observed (Fig. 6d). Besides, neither remarkable body weight loss nor abnormal behavior occurred in the treatment groups compared to the controls (Fig. 6c). All the above results consistently confirm that the developed PLNP-BAC-PEGBT platform is competent for tumor-specific ablation by a single intravenous injection and one-time continuous or even fractionated laser irradiation with good therapeutic effects and no obvious side-effects.

Conclusions

In summary, we have reported a PLNP-BAC-PEGBT theranostic nanoplatform based on pH-reversibly activatable NIR PTT/PDT-in-one agent BAC and NIR renewable nanoimplant PLNPs for precision tumor-targeting and autofluorescence-free image-guided efficient phototherapy without the need for continuous external irradiation. The reversibly activatable PTT/PDT synergetic enhancement effect of BAC in combination with the super-long NIR afterglow feature of PLNPs makes the PLNP-BAC-PEGBT effectively overcome the shortcomings of limited therapeutic efficiency and non-specific damage in the previous 'always on' or irreversible 'turn-on' PTT/PDT platforms with the need for continuous and long term *in situ* irradiation. Such a pH-reversibly activatable PTT/PDT synergetic effect, needless continuous external laser irradiation and BT-mediated active targeting combined with autofluorescence-free NIR image-guiding endow the smart theranostic nanoplatform with great potential for precision tumor-targeting and excellent therapeutic effects without nonspecific damage. This work furnishes a prospective strategy to design an intelligent theranostic platform for precision medicine.

Ethical statement

All experiments were performed in strict accordance with the Chinese National Standard Laboratory animal Guideline for the ethical review of animal welfare (GB/T 35892-2018) and were approved by the Institutional Animal Care and Use Committee of Jiangnan University (Wuxi, China).

Conflicts of interest

There are no conflicts to declare.

Acknowledgements

The authors appreciate the support from the National Natural Science Foundation of China (No. 21934002, 21804056 and 21804057), the Natural Science Foundation of Jiangsu Province, China (No. BK20180581 and BK20180584), the China Postdoctoral Science Foundation (No. 2018M630511 and 2018M630509), the National First-class Discipline Program of Food Science and Technology (No. JUFSTR20180301), and the Collaborative Innovation Center of Food Safety and Quality Control in Jiangsu Province.

Notes and references

1 W. Xiao, P. Wang, C. Ou, X. Huang, Y. Tang, M. Wu, W. Si, J. Shao, W. Huang and X. Dong, *Biomaterials*, 2018, **183**, 1–9.
2 G. Lan, K. Ni and W. Lin, *Coord. Chem. Rev.*, 2019, **379**, 65–81.
3 J. F. Lovell, T. W. B. Liu, J. Chen and G. Zheng, *Chem. Rev.*, 2010, **110**, 2839–2857.
4 L. Y. Li, Y. M. Zhou, R. Y. Gao, X. C. Liu, H. H. Du, J. L. Zhang, X. C. Ai, J. P. Zhang, L. M. Fu and L. H. Skibsted, *Biomaterials*, 2019, **190–191**, 86–96.
5 C. Wang, B. Huang, G. Yang, Y. Ouyang, J. Tian and W. Zhang, *Biomacromolecules*, 2019, **20**, 4218–4229.
6 W. Fan, W. Bu, B. Shen, Q. He, Z. Cui, Y. Liu, X. Zheng, K. Zhao and J. Shi, *Adv. Mater.*, 2015, **27**, 4155–4161.
7 Y. Cheng, H. Cheng, C. Jiang, X. Qiu, K. Wang, W. Huan, A. Yuan, J. Wu and Y. Hu, *Nat. Commun.*, 2015, **6**, 8785.
8 P. Li, L. Liu, Q. Lu, S. Yang, L. Yang, Y. Cheng, Y. Wang, S. Wang, Y. Song, F. Tan and N. Li, *ACS Appl. Mater. Interfaces*, 2019, **11**, 5771–5781.
9 M. Sun, L. Xu, W. Ma, X. Wu, H. Kuang, L. Wang and C. Xu, *Adv. Mater.*, 2016, **28**, 898–904.
10 B. Tian, C. Wang, S. Zhang, L. Feng and Z. Liu, *ACS Nano*, 2011, **5**, 7000–7009.
11 X. Hu, H. Tian, W. Jiang, A. Song, Z. Li and Y. Luan, *Small*, 2018, **14**, 1802994.
12 Y. K. Kim, H. K. Na, S. Kim, H. Jang, S. J. Chang and D. H. Min, *Small*, 2015, **11**, 2527–2535.
13 X. Li, S. Kolemen, J. Yoon and E. U. Akkaya, *Adv. Funct. Mater.*, 2017, **27**, 1604053.
14 X. Li, S. Lee and J. Yoon, *Chem. Soc. Rev.*, 2018, **47**, 1174–1188.
15 Q. Zhan, J. Qian, H. Liang, G. Somesfalean, D. Wang, S. He, Z. Zhang and S. Andersson-Engels, *ACS Nano*, 2011, **5**, 3744–3757.
16 G. Yang, D. Yang, P. Yang, R. Lv, C. Li, C. Zhong, F. He, S. Gai and J. Lin, *Chem. Mater.*, 2015, **27**, 7957–7968.
17 S. K. Sun, H. F. Wang and X. P. Yan, *Acc. Chem. Res.*, 2018, **51**, 1131–1143.
18 Y. Li, M. Gecevicius and J. Qiu, *Chem. Soc. Rev.*, 2016, **45**, 2090–2136.
19 T. Maldiney, A. Lecointre, B. Viana, A. Bessière, M. Bessodes, D. Gourier, C. Richard and D. Scherman, *J. Am. Chem. Soc.*, 2011, **133**, 11810–11815.
20 Z. Pan, Y. Y. Lu and F. Liu, *Nat. Mater.*, 2011, **11**, 58–63.
21 Z. Li, Y. Zhang, X. Wu, X. Wu, R. Maudgal, H. Zhang and G. Han, *Adv. Sci.*, 2015, **2**, 1500001.
22 Z. Li, Y. Zhang, X. Wu, L. Huang, D. Li, W. Fan and G. Han, *J. Am. Chem. Soc.*, 2015, **137**, 5304–5307.
23 W. Fan, N. Lu, C. Xu, Y. Liu, J. Lin, S. Wang, Z. Shen, Z. Yang, J. Qu, T. Wang, S. Chen, P. Huang and X. Chen, *ACS Nano*, 2017, **11**, 5864–5872.
24 R. Abdurahman, C. X. Yang and X. P. Yan, *Chem. Commun.*, 2016, **52**, 13303–13306.
25 J. Wang, Y. Li, R. Mao, Y. Wang, X. Yan and J. Liu, *J. Mater. Chem. B*, 2017, **5**, 5793–5805.

26 Y. J. Li, C. X. Yang and X. P. Yan, *Anal. Chem.*, 2018, **90**, 4188–4195.
27 L. Hu, P. Wang, M. Zhao, L. Liu, L. Zhou, B. Li, F. H. Albaqami, A. M. El-Toni, X. Li, Y. Xie, X. Sun and F. Zhang, *Biomaterials*, 2018, **163**, 154–162.
28 Y. J. Li and X. P. Yan, *Nanoscale*, 2016, **8**, 14965–14970.
29 J. Wang, Q. Ma, X. X. Hu, H. Liu, W. Zheng, X. Chen, Q. Yuan and W. Tan, *ACS Nano*, 2017, **11**, 8010–8017.
30 B. B. Srivastava, A. Kuang and Y. Mao, *Chem. Commun.*, 2015, **51**, 7372–7375.
31 E. Teston, S. Richard, T. Maldiney, N. Lièvre, G. Y. Wang, L. Motte, C. Richard and Y. Lalatonne, *Chem.-Eur.J.*, 2015, **21**, 7350–7354.
32 J. Jiang, Z. Zhao, Z. Hai, H. Wang and G. Liang, *Anal. Chem.*, 2017, **89**, 9625–9628.
33 X. Li, C. Y. Kim, S. Lee, D. Lee, H. M. Chung, G. Kim, S. H. Heo, C. Kim, K. S. Hong and J. Yoon, *J. Am. Chem. Soc.*, 2017, **139**, 10880–10886.
34 F. Hu, S. Xu and B. Liu, *Adv. Mater.*, 2018, **30**, 1801350.
35 J. Cao, J. Chi, J. Xia, Y. Zhang, S. Han and Y. Sun, *ACS Appl. Mater. Interfaces*, 2019, **11**, 25720–25729.
36 E. Boedtkjer and S. F. Pedersen, *Annu. Rev. Physiol.*, 2020, **82**, 103–126.
37 B. P. Lin, H. T. Chen, D. Y. Liang, W. Lin, X. Y. Qi, H. P. Liu and X. Y. Deng, *ACS Appl. Mater. Interfaces*, 2019, **11**, 11157–11166.
38 Z. Sheng, D. Hu, M. Zheng, P. Zhao, H. Liu, D. Gao, P. Gong, G. Gao, P. Zhang, Y. Ma and L. Cai, *ACS Nano*, 2014, **8**, 12310–12322.
39 M. Zheng, P. Zhao, Z. Luo, P. Gong, C. Zheng, P. Zhang, C. Yue, D. Gao, Y. Ma and L. Cai, *ACS Appl. Mater. Interfaces*, 2014, **6**, 6709–6716.
40 W. S. Kuo, Y. T. Chang, K. C. Cho, K. C. Chiu, C. H. Lien, C. S. Yeh and S. J. Chen, *Biomaterials*, 2012, **33**, 3270–3278.
41 F. Liu, Y. Chen, Y. Liang and Z. Pan, *Opt. Lett.*, 2016, **41**, 954–957.
42 R. Kumar, E. J. Kim, J. Han, H. Lee, W. S. Shin, H. M. Kim, S. Bhuniya, J. S. Kim and K. S. Hong, *Biomaterials*, 2016, **104**, 119–128.
43 X. Li, C. Y. Kim, S. Lee, D. Lee, H. M. Chung, G. Kim, S. H. Heo, C. Kim, K. S. Hong and J. Yoon, *J. Am. Chem. Soc.*, 2017, **31**, 10880–10886.
44 D. N. Heo, D. H. Yang, H. Moon, J. B. Lee, M. S. Bae, S. C. Lee, W. J. Lee, I. C. Sun and I. K. Kwon, *Biomaterials*, 2012, **33**, 856–866.